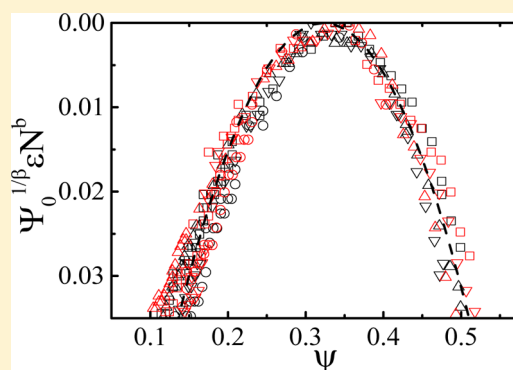


## Mapping Phase Diagrams of Polymer Solutions by a Combination of Microfluidic Solution Droplets and Laser Light-Scattering Detection

Yonggang Shangguan,<sup>†,§,\*</sup> Dameng Guo,<sup>†</sup> Hui Feng,<sup>†</sup> Yuan Li,<sup>†</sup> Xiangjun Gong,<sup>†</sup> Qianjin Chen,<sup>†</sup> Bo Zheng,<sup>†,\*</sup> and Chi Wu<sup>†,‡,\*</sup><sup>†</sup>Department of Chemistry, The Chinese University of Hong Kong, Shatin, N.T., Hong Kong<sup>‡</sup>Hefei National laboratory of Physical Science at Microscale, Department of Chemical Physics, The University of Science and Technology of China, Hefei, Anhui 230026, China<sup>§</sup>MOE Key Laboratory of Macromolecular Synthesis and Functionalization, Department of Polymer Science and Engineering, Zhejiang University, Hangzhou 310027, China

**ABSTRACT:** Conventional mapping of a phase diagram of a polymer in a solvent requires a substantial amount of polymer (e.g., at least of the order of ~100 mg of narrowly distributed samples with different molar masses) and may take months or even years to reach the true two phase equilibrium at each given temperature, especially when the polymer concentration is high. This is why good phase diagrams of polymer solutions are rare in the literature. To solve such a problem, we developed a Teflon microfluidic device to prepare and store a series of droplets (~10 nL) at different polymer concentrations inside a glass capillary. The phase transition inside each polymer solution droplet sealed and isolated in immiscible fluorohydrocarbon could be quickly and precisely monitored by a newly developed small angle laser light scattering detector. Using poly(vinyl acetate) (PVAc) in isobutyl alcohol and in benzene as two examples, we demonstrated that a combination of microfluidic device and small angle light scattering enables us to map the phase diagram of a polymer in a given solvent within hours by using only a few mg of the sample because (1) each droplet contains no more than ~10 μg polymer and (2) the phase-transition induced interchain association inside each droplet can be quickly and sensitively detected. We have demonstrated that two sets of a total of eight precisely mapped phase diagrams of four PVAc fractions in the two solvents can be reasonably scaled together to form a master curve.



## INTRODUCTION

A well-defined phase diagram of a polymer in a given solvent is not only fundamentally important but also useful in various applications, including polymer preparation, purification, and characterization.<sup>1–3</sup> Despite its importance, only few good phase diagrams of polymer solutions have been reported so far, such as polystyrene and poly(methyl methacrylate) in a limited number of solvents even though polymer science has been developed as a research field for a long time.<sup>4–6</sup> Two major issues have hindered precise mapping of a phase diagram of a polymer in a given solvent. The first is that the polymer phase diagram depends on the chain length, different from the phase diagram of small molecular solutions, so that one has to first obtain a series of narrowly distributed samples at different molar masses. Most of synthetic polymers are very broadly distributed in their molar masses. One can certainly fractionate such a sample into a set of narrowly distributed ones with different molar masses but the conventional method requires ~1 mL polymer solution with a concentration at or near its critical concentration that depends on the molar mass, i.e., more than few hundred milligrams of a narrowly distributed sample, which makes the sample preparation rather difficult.

The second issue is more detrimental, i.e., the extremely long experimental time. In a typical experiment of mapping the phase diagram, one alternates the solution temperature to induce the phase transition and has to wait until the solution has reached its thermodynamic equilibrium at which stage the solution separates into one polymer-rich phase and another solvent-rich phase; and finally determines the polymer concentrations in the two phases normally by a refractive index method. By repeating the last two steps, the phase diagram can be in principle mapped even it is a painful process. In reality, the translational diffusion of long polymer chains in concentrated polymer solutions (e.g., polystyrene with  $M \sim 10^5$ – $10^6$  g/mol in benzene, 0.1–0.2 v/v) is extremely slow with a typical translational diffusion coefficient of  $10^{-8}$ – $10^{-9}$  cm<sup>2</sup>/s or even slower; i.e., it would take ~months to years for an entangled long chain in a concentrated solution to enter or leave the solution phase and move a macroscopic distance of even 5 mm. Thus, it is impractical for a concentrated polymer

Received: January 7, 2014

Revised: March 2, 2014

Published: March 20, 2014

solution to reach its true equilibrium during the phase separation within a reasonable time period. Moreover, one will never be sure whether the two phases have reached their thermodynamic equilibrium.

Consequently, in order to practically map the phase diagram of a polymer solution, one has to use a much smaller volume of polymer solution to reduce the amount of sample used and the measurement time required in each measurement. In this aspect, the microfluidic platform developed in recent years enables us to simultaneously solve these two problems. Previously, the microfluidic devices have already been used to study the phase behavior and other properties of macromolecules.<sup>7–15</sup> Cremer and co-workers<sup>7,8</sup> developed a microfluidic device to quickly measure the phase separation temperature of thermally sensitive polymer solutions stored in a glass capillary. However, in their method, a series of polymer solutions at different concentrations has to be prepared and inserted into the capillary individually, which makes the sample preparation and experiments extremely time-consuming.

On the other hand, various on-chip methods have been recently developed to concentrate or dilute a given solution. In the on-chip approach, the water permeability of poly-(dimethylsiloxane) (PDMS) elastomer was exploited by alternating the concentration in aqueous solutions. For example, a microfluidic device, denoted as the *Phase Chip*, was fabricated to investigate the phase transition of the PEG/salt aqueous mixture and protein crystallization,<sup>12</sup> and a microchamber-based single-layer microfluidic device was developed to study the phase separation of PNIPAM in aqueous solutions.<sup>13</sup> The main disadvantage of such devices is that the water evaporation through PDMS takes a long time to reach a desired concentration during sample preparation. In comparison, on-chip dilution is faster and has few approaches.

Hansen et al.<sup>9</sup> developed an integrated microfluidic device to rapidly generate a number of nanoliter protein solutions at different concentrations so that they could further study the protein phase behavior. Laval et al.<sup>11</sup> generated a series of nanoliter on-chip droplets at different concentrations of adipic acid and studied their phase diagram. Using the on-chip droplet method and a PDMS/glass capillary microfluidic device, Shi et al.<sup>10,15,16</sup> generated an array of PNIPAM-solution droplets at different concentrations and estimated their phase diagram. These on-chip methods have two shortcomings as follows: (1) PDMS devices used are only good for aqueous solutions but most of polymers are only soluble and can be characterized and processed in organic solvents. (2) CCD used to detect the phase separation is not sufficiently sensitive.

To address these two issues, we decided to fabricate a microfluidic device made of Teflon so that it can take any solvent to generate a series of nanoliter polymer-solution droplets at different concentrations. Teflon was used because of its superior chemical resistance to nearly all solvents, including organic ones and also because of its low interfacial energy with fluorohydrocarbons used to isolate each polymer-solution droplet.<sup>14</sup> At the same time, we developed a sensitive small-angle laser light-scattering detection system to effectively monitor the phase transition in each droplet. In the current study, we used four fractions of narrowly distributed poly(vinyl acetate) at different molar masses and two different solvents (isobutyl alcohol and benzene) to demonstrate the principle of how to quickly and accurately map the phase diagram of a given polymer solution.

## EXPERIMENTAL SECTION

**Materials.** A commercial poly(vinyl acetate) (PVAc,  $M_w = 2.56 \times 10^5$  and PDI = 2.39) sample was purchased from Sigma-Aldrich. Isobutanol (IBA) and benzene were obtained from Mallinckrodt and Sigma-Aldrich, respectively, and used without further purification. A semicrystalline Teflon plate, perfluoroalkoxy (PFA), with an approximate thickness of 1.0 mm was purchased from Yuyisong, Inc. Photoresist (SU-8) and PDMS prepolymer were respectively purchased from Microchem and Dow Corning (Sylgard 184). Fluorocarbon oil (FC3283) and a fluoro-surfactant (1H,1H,2H,2H-perfluoro-1-octanol, PFO) were obtained from 3 M and Sigma-Aldrich, respectively.

**Fractionation.** Four fractions of narrowly distributed PVAc samples were obtained from its acetone solution at 35 °C by a successive slow addition of water. The procedure is outlined as follows. After water as a precipitant was slowly added into a stirring PVAc solution in acetone that contained 2.0 g PVAc at 35 °C until it became slightly turbid, the solution mixture was slowly heated to make it clear and then was cooled down to 35 °C under gentle stirring. The solution mixture was allowed to stand overnight without any disturbance. The insoluble high molar mass fraction was settled down at the bottom, separated by decantation, and washed with deionized water before it was first dried in a steam bath and then in vacuum at 50 °C. By repeating such a procedure, we obtained a series of narrowly distributed PVAc fractions with decent molar masses. The number- and weight-average molar masses and the degree of polymerization of four of them used in the current study are summarized in Table 1.

**Table 1.** Number and Weight Average Molar Masses ( $M_n$  and  $M_w$ ) and Degree of Polymerization ( $N$ ) of Four PVAc Fractionations Used in the Current Study, Where  $M_0$  is Molar Mass of Monomer

PVAc sample	$M_n$ (g/mol)	$M_w$ (g/mol)	$N = M_n/M_0$
PVAc-1	$1.71 \times 10^4$	$1.98 \times 10^4$	$2.0 \times 10^2$
PVAc-2	$4.93 \times 10^4$	$6.26 \times 10^4$	$5.7 \times 10^2$
PVAc-3	$1.74 \times 10^5$	$2.11 \times 10^5$	$2.0 \times 10^3$
PVAc-4	$4.57 \times 10^5$	$6.13 \times 10^5$	$5.3 \times 10^3$

**Teflon Microfluidic device.** It has a dimension of 1 cm  $\times$  6 cm and was fabricated by hot embossing,<sup>14</sup> as schematically shown in Figure 1. The fabrication process is outlined as follows: (1) a PDMS

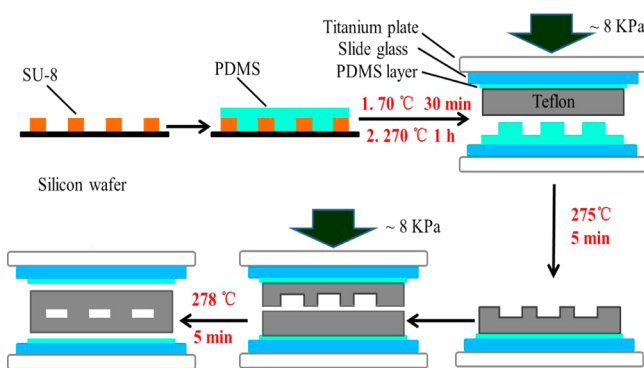


**Figure 1.** Schematic of how a Teflon microfluidic device is made by hot embossing.

mold was fabricated with the complementary relief structure by soft lithography;<sup>17</sup> (2) the mold was placed on a glass slide and annealed at 270 °C in an oven for ~1 h to improve its mechanical strength; (3) the PFA substrate was sandwiched between the PDMS mold and another glass slide coated with a thin PDMS layer; (4) the assembled sandwich was placed inside a hot compressor (TM-101F, Taiming, Inc.) to be embossed at 275 °C for 5 min and then cooled down to room

temperature under a pressure of  $\sim 8$  kPa so that the desired pattern was transferred into the PFA slab; and (5) the complete Teflon microdevice was assembled by bonding the embossed PFA slab with another flat PFA slab. Note that before the bonding at  $278$  °C for 5 min, several holes were drilled through the PFA slab for reservoirs and tube connections; the PFA slabs were cleaned by acetone and blow-dried. The obstruction and leakage of such a prepared microchannel in the Teflon device were checked by the fluorocarbon oil flow.

**Preparation of Droplets.** Each PVAc sample was dissolved in isobutyl alcohol or benzene at a higher temperature with an initial concentration in the range 0.1–0.6 v/v, depending on its molar mass. To ensure the formation and transportation of polymer-solution droplets inside the microchannel, we used fluorohydrocarbon FC3283 (refractive index,  $n = 1.29$ ) with 0.1 wt % of PFO as the carrier fluid. The microchannel was connected to a borosilicate glass capillary (Vitrocom) via a Teflon tube (an internal diameter of 0.3 mm) so that the droplets can be transported and stored inside the capillary ( $n = 1.47$ ) with an inner square cross-section ( $200 \times 200 \mu\text{m}^2$ ), as shown in Figure 2. Note that the device has a size of 10 mm  $\times$  60 mm with a

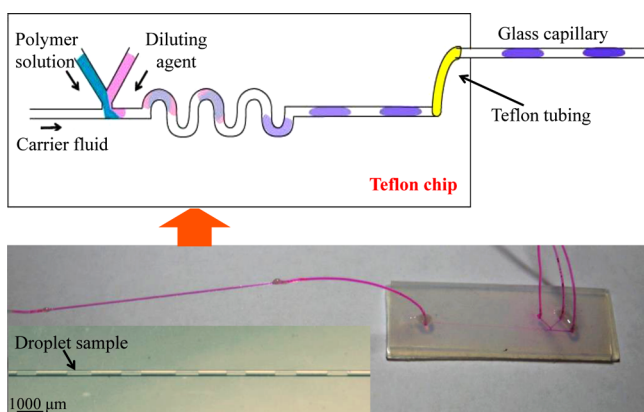


**Figure 2.** Schematic of how droplets were fabricated in a Teflon microfluidic device.

height of  $200 \mu\text{m}$ . The whole process was controlled by a Labview program.<sup>15,16</sup> The flow rate of FC3283 was kept constant at  $1.00 \mu\text{L}/\text{min}$ . A typical initial flow rate of the PVAc solution was in the range of  $0.40$ – $0.80 \mu\text{L}/\text{min}$ , depending on the initial polymer concentration. Using a lower initial polymer concentration (PVAc1, 0.5; PVAc2, 0.4; PVAc3, 0.3; and PVAc4, 0.2 v/v), we could generate 40 droplets,

where the flow rate of the PVAc solution started at  $0.78 \mu\text{L}/\text{min}$  with a ramp rate and time of  $-0.019 \mu\text{L}/\text{min}$  and 39 s; and the step duration of 1 s; while the initial flow rate of the diluting agent (solvent) was  $0.02 \mu\text{L}/\text{min}$  with a ramp rate of  $0.019 \mu\text{L}/\text{min}$ . In contrast, using a higher initial polymer concentration (PVAc1, 0.6; PVAc2, 0.48; PVAc3, 0.4; and PVAc4, 0.3, v/v), we were only able to generate 10 droplets, where the initial flow rate of PVAc solution was  $0.36 \mu\text{L}/\text{min}$  with a ramp rate and time of  $-0.032 \mu\text{L}/\text{min}$  and 59 s, respectively, and the step duration of 6 s; while the flow rate of the diluting agent (solvent) started at  $0.04 \mu\text{L}/\text{min}$  with a ramp rate and time of  $0.032 \mu\text{L}/\text{min}$  and 59 s, respectively. Such generated polymer solution droplets were directly transported to the capillary and stored with its two ends sealed with glue for mapping the phase diagram of polymer solutions.

**Phase Transition Measurement.** After a polymer solution was moved from the one-phase to the two-phase regime, polymer chains started to undergo the interchain association but the polymer solution might remain transparent and clear for a long time so that the turbidity measurement was less sensitive than laser light scattering (LLS) because (1) the scattered light intensity ( $\langle I \rangle$ ) was typically only  $10^{-4}$  of the incident light intensity so that the transmitted light intensity changed little when the solution was still transparent but the chains already started to aggregate with one another;<sup>18</sup> and (2) the scattered light intensity at a low scattering angle was proportional to the square of the mass of a scattering objective; namely, an aggregate with 10 chains should scatter 100 times of light than that from an individual chains. This was the reason why we developed a low-angle LLS detection system to monitor the phase transition inside each droplet, as shown in Figure 3.

In such a device, a He–Ne laser (JDSU-1507P) and a photodiode (S2386, Hamamatsu) was used as the light source and detector, respectively. To obtain a suitable size and length of the focused spot for the optimal measurement (Supporting Information), we used a laser beam expander (20 $\times$ , Edmund) and a convex lens with a focal length of 300 mm to adjust the optical path. The diode detector was placed at  $\sim 4.3^\circ$ . A copper block with a slot to fit the glass capillary that contained a series of droplets at different concentrations is thermally controlled by a circulator (Julabo F32-EH). The actual temperature of the glass capillary was monitored by a small thermocouple meter (Sable systems international, TC-2000). The gap between the slot and the capillary was further filled with a degassed PDMS prepolymer (the weight ratio of component A and B was 5:1) and heated to  $65$  °C in an oven for  $\sim 2$  h so that the capillary was surrounded by PDMS to improve its thermal conductivity and to reduce the background scattering from the glass capillary itself. Before mapping the phase diagram, the brass block with the glass capillary was heated to  $60$  °C to

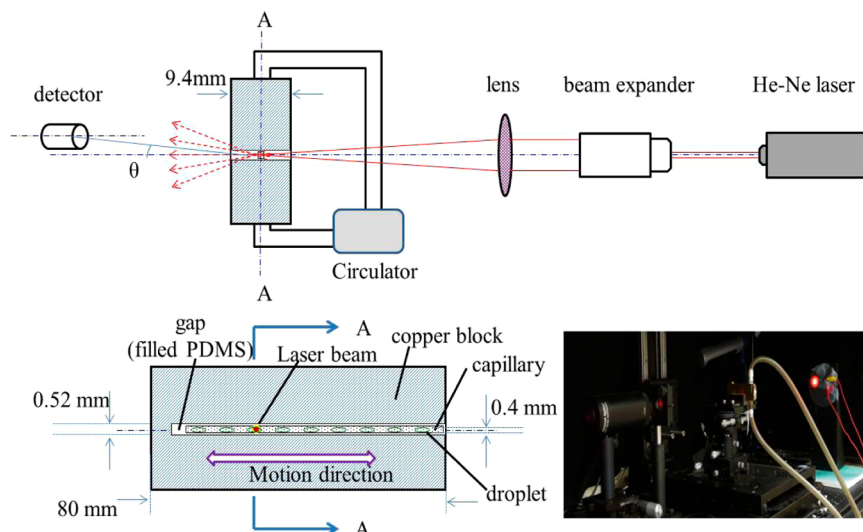


**Figure 3.** Schematic of home-built low-angle laser light scattering device for monitoring the phase transition of polymer solution inside each droplet.

ensure that polymer solutions inside all the droplets were in the one-phase regime. The temperature fluctuation was less than 0.02 °C. The brass block with the capillary is fixed on a moving platform that is driven by a computer-controlled stepping micromotor (MC300, Zolix) with a linear displacement. In the droplet-scanning mode, for a given temperature, each droplet can be driven to pass the incident laser beam so that its scattered light intensity is recorded. For comparison, we also used the temperature-scanning mode, i.e., by fixing the laser beam on one droplet (concentration), we ramped the solution temperature to find its phase transition temperature before moving to another droplet. The heating/cooling rate between different temperatures was controlled in the range 0.1–2 °C/min.

## RESULTS AND DISCUSSION

**Generation of Droplets with Gradient at Different Polymer Concentrations.** After several tries, we found that fluorohydrocarbon FC3283 with 0.1 wt % PFO was an excellent carrier for an easy formation of polymer solution droplets inside the Teflon microchannel and the glass capillary.<sup>19</sup> To map the phase diagram of a polymer solution, it was vitally important for us to know the concentration inside each droplet. Here, we used a fluorescent internal marker, Rhodamine 6G. A comparative study between PVAc solutions with and without Rhodamine 6G confirmed that the marker had no observable effect on the phase transition of PVAc solutions and PVAc produced a negligible difference in the fluorescence of Rhodamine 6G.

Figure 4 shows the fluorescence intensity of such successively prepared 40 droplets, which were measured using a confocal

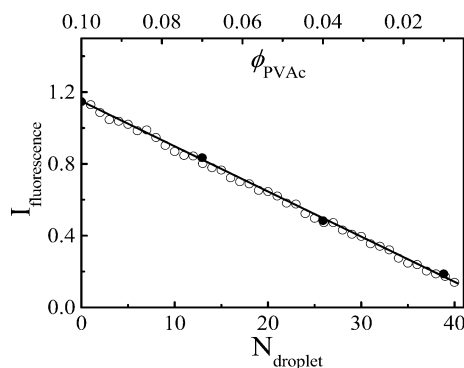


**Figure 4.** Polymer concentration dependence of fluorescence intensities of droplets of PVAc1 in isobutyl alcohol with different amounts of Rhodamine 6G, which is directly correlated to polymer concentration, where filled symbols represents fluorescence intensities of Rhodamine 6G in isobutyl alcohol without PVAc but predetermined concentrations, where volume concentration uncertainty of each droplet is no more than  $\pm 0.001$  v/v.

laser scanning microscope. The fluorescence intensity of Rhodamine 6G inside these solution droplets decreased linearly with increasing droplet number index, i.e., the no. 1 droplet had the highest Rhodamine 6G concentration while no. 40 had the lowest one. The PVAc concentration inside each droplet was correlated to the fluorescence intensity because Rhodamine 6G was added in the initial PVAc solution with a concentration of 200 ppm. To confirm such correlation between polymer concentration and fluorescence intensity, the initial polymer solution with Rhodamine 6G was diluted to three known concentrations and their fluorescence intensities were measured as references (filled symbols). Figure 4 demonstrates that we can use the Teflon microfluidic device to prepare a series of

droplets with a well-controlled polymer concentration gradient. After establishing such a series of small polymer solution droplets at different polymer concentrations, we are able to use either a temperature-scanning mode or a droplet-scanning mode to find the points ( $\phi_P$  and  $T_P$ ) on the coexistence curve.

Figure 5 shows that in the temperature-scanning mode, the relative scattered light intensity ( $\langle I \rangle_R$ ) of one droplet suddenly

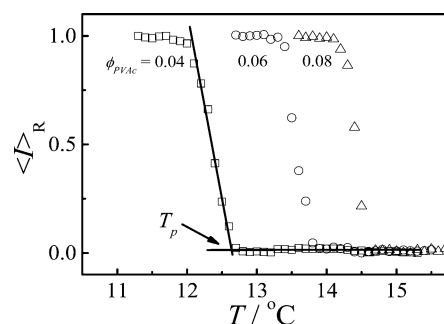


**Figure 5.** Temperature dependence of relative intensity of three droplets of PVAc1 in IBA prepared with an initial volume concentration of  $\phi_{PVAc} = 0.1$ .

increased when the temperature was decreased to a point, where the scattered light intensity had been normalized by  $\langle I \rangle_R = (\langle I \rangle - \langle I \rangle_0) / (\langle I \rangle_{max} - \langle I \rangle_0)$  with  $\langle I \rangle$ ,  $\langle I \rangle_0$  and  $\langle I \rangle_M$  being the intensities measured at  $T$ , in the one-phase regime and in the two-phase regime, respectively. The normalization removed the difference in the polymer concentration of different droplets so that we could compare their relative intensity change. The abrupt change of  $\langle I \rangle_R$  marked the phase transition temperature ( $T_P$ ), as indicated by the intersection of two tangents. Note that such obtained  $T_P$  depended slightly on the cooling rate in the range 0.1–1.0 °C/min; namely, the slower the rate, the lower the measured  $T_P$ . Therefore, it is worth noting that many so-called “phase diagrams” of polymer solutions in the literature were simply mapped by using the temperature-ramping turbidity measurements. Besides the problem of the ramping rate just mentioned, the turbidity occurred often well after the solution had passed the true phase transition temperature on the coexistence curve so that the entire coexistence curve was pushed down for a solution with an upper critical solution temperature. The slowest scanning rate (0.1 °C/min) was limited by the accuracy of our current thermostat used. In principle, there should be no problem to slow it down in order to make it more accurate. In contrast, in the droplet-scanning mode, we scanned and measured the scattered light intensity of different droplets for a given  $T$ .

Figure 6 shows that for a given solution temperature, the weight concentration corrected normalized scattered light intensity nearly remains constant until the polymer solution enters the two phase regime in which the scattered light intensity sharply increases, where for the droplets with different concentrations, the equilibration time required ranges between 20 and 100 s but the time interval between the measurements at two temperatures was 20 min, much longer than that is required to reach the equilibration. Note that the change is so sharp that we can accurately determine the two points on the coexistence curve ( $\phi_L$  and  $\phi_H$ ) for a given temperature from the intersections of two near vertical lines with two lower near horizontal lines. In the current study, the temperature interval (step) used was 0.1 °C. Note that the values of  $T_P$  obtained in

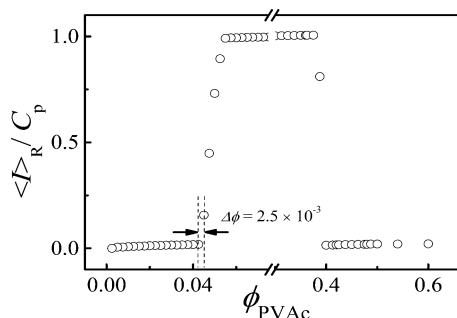


**Figure 6.** Polymer volume concentration dependence of weight concentration ( $C_p$ ) corrected normalized scattered light intensity ( $(I)_R/C_p$ ) at 13.0 °C, where the temperature uniformity was within 0.02 °C.

such a way were slightly higher than those from the temperature scanning mode but close to those obtained with the slowest scanning rate of 0.1 °C/min because in the droplet-scanning mode, there was no temperature change during each droplet scanning, i.e., it could be considered as an infinitely slow temperature scanning. On the other hand, there existed a small difference between temperature readings of the thermal probe and the thermostat. The faster the temperature scanning rate, the larger the difference is. Therefore, the droplet-scanning mode is better and more accurate. Also note that the two intersections with the up horizontal line might lead to two points on the spinodal curve.

It should be emphasized that there was no need for us to wait for the phase separation inside each droplet to reach its thermodynamic equilibrium before measuring the scattered light intensity. Instead, for each given temperature, we used the very sensitive LLS method to scan all the droplets and find in which droplet (concentration) range the scattered light intensity rose, signaling the association of polymer chains, which led to  $\phi_L$  and  $\phi_H$  on the coexistence curve. By changing the solution temperature in a small step of 0.1 °C and repeating the droplet-scanning procedure, we were able to quickly map the phase diagram of a polymer solution, as shown in Figure 7.

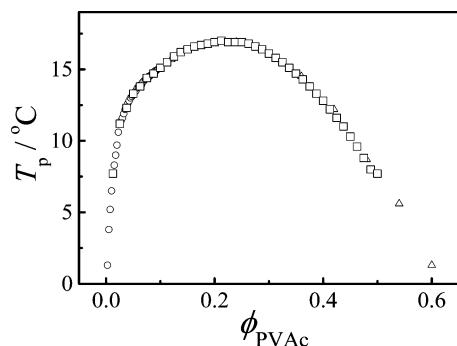


**Figure 7.** Polymer volume concentration ( $\phi_{PVAc}$ ) dependence of phase transition temperature ( $T_p$ ) of PVAc1 in IBA.

It should be stated that in Figure 7, in order to prepare the polymer solution droplets over a wide concentration range 0.0025–0.6 (v/v), we used three PVAc solutions with different initial concentrations to make 40 droplets. The cross-section of each droplet is 200  $\mu\text{m}$   $\times$  200  $\mu\text{m}$  and the average length of the droplets was  $\sim$ 400  $\mu\text{m}$ . Using this method, we were able to conveniently prepare a large number of droplets with a small

concentration interval. Figure 7 shows that some of the data points from the three series of droplets are overlapped with each other very well, indicating the accuracy and validity of our droplet-based method. As expected, the PVAc1 in isobutyl alcohol has an upper critical solution temperature (UCST) and its phase diagram is asymmetric with a critical point located at  $\phi_{PVAc,C} = 0.21$  and  $T_C = 17.0$  °C.

On the other hand, it is well-known that the chain length remarkably influences the phase diagram of a polymer solution.<sup>4</sup> Therefore, it is important to determine the chain-length dependent phase diagram for a polymer in a given solvent. In the currently developed droplet method, we only need a small amount of sample (a few milligrams) to map a phase diagram. It is not so difficult to use the conventional precipitation-fractionation or GPC method to obtain a small amount of narrowly distributed polymer samples at different molar masses and then map the phase diagram of each of such obtained fractions. Figure 8 shows the polymerization degree

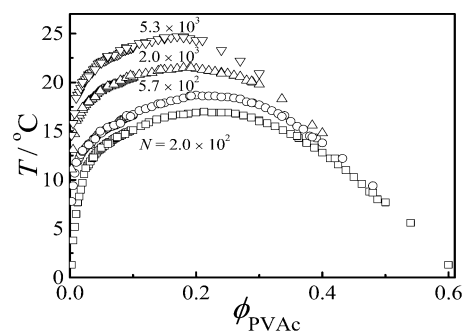


**Figure 8.** Chain-length dependence of phase diagram of PVAc in isobutyl alcohol.

(chain length) dependence of the phase diagrams of PVAc in isobutyl alcohol, where each phase diagram was obtained from three series of droplets prepared from three initial PVAc solutions with different polymer concentrations. It shows that such prepared three sets of data overlap with each other very well in each phase diagram.

As expected, each phase diagram shifts to a higher temperature and toward the lower concentration as the chain length increases because the asymmetric size difference between a polymer chain and a solvent molecule. Note that it would take years to obtain such precise chain-length dependent phase diagrams if using the conventional refractive index method to measure  $\phi_L$  and  $\phi_H$  after the two phases reached the equilibrium for a given temperature. To our knowledge, these are the first reported good phase diagrams of PVAc in isobutyl alcohol. An attentive reader might find that the highest polymer concentration used to construct the phase diagram decreases as the chain length increases. This is mainly because the solution viscosity increased with the chain length so that it was difficult to use the microfluidic device to prepare the droplets with a viscous polymer solution, a practical limitation.

Furthermore, using the same procedure, we mapped the phase diagrams of different PVAc samples in one additional solvent, benzene, as shown in Figure 9. It should be stated that benzene is slightly soluble in FC3283, but such a low solubility has no effect on the polymer concentration and properties inside the droplets. As expected, the phase diagrams of PVAc in benzene and in isobutyl alcohol have a similar feature, but the

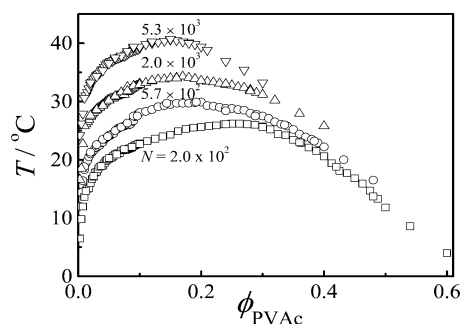


**Figure 9.** Chain-length dependence of phase diagrams of PVAc in benzene.

upper critical solution temperature of PVAc in benzene is much higher, indicating that isobutyl alcohol is a better solvent than benzene for a given temperature. Since the droplet-preparation device is made of Teflon and glass, we, in principle, could use it to prepare polymer droplets at even higher temperatures, which would reduce the solution viscosity, i.e., increase the concentration range for longer polymer chains. Practically, as long as a polymer solution is able to completely flow down in  $\sim 30$  min under gravity when its container is inverted, one will be able to prepare the droplets by using our new Teflon microfluidic device and map the phase diagram.

The asymmetry of polymer phase diagrams is due to a huge size difference between a long polymer chain and a solvent molecule. In order to account such a size effect, one can define a new dimensionless order parameter ( $\Psi$ ) as<sup>20</sup>

$$\Psi = \frac{\phi_p}{\phi_p + R_c(1 - \phi_c)} \quad (1)$$

where  $R_c$  is a chain-length dependent constant that reflects the “size” ratio of polymer chain and solvent molecule. Here, one should not take the “sizes” literally because they include the intermolecular interaction. The phase diagram can be symmetrized as

$$|\Psi - \Psi_c| = \Psi_0(\epsilon N^b)^\beta \quad (2)$$

where  $\Psi_c$ ,  $\Psi_0$ ,  $b$ , and  $\beta$  are constants, independent of the chain length. Figure 10 shows such symmetrized phase diagrams, respectively, from Figures 8 and 9 with those listed parameters.

It is interesting to note that in each solvent, the phase diagrams of four PVAc samples are collapsed into a master curve after such a symmetrized operation even though the data points are slightly scattered over a small range, where we have used a criteria of  $\epsilon_{\max} N^{0.3} < 0.075$ , i.e., those data points close to  $T_c$  because it defines the scaling range.<sup>20</sup> Also note that the values of  $\Psi_c$ ,  $b$  and  $\beta$  are independent of the solvent used except  $\Psi_0$ . In theory,  $\beta = 1/3$ , a constant for linear chains in good solvents,<sup>21</sup> which has also been experimentally confirmed.<sup>22,23</sup> Here, our fitted value of  $\beta$  is larger than the expected one and close to  $1/2$  predicted by the mean-field theory. On the other hand, the value of  $b$  is much lower than those predicted before, which might be attributed to the fact that the molar mass distributions of these samples used are not sufficiently narrow and the overestimated or inaccurate average molar masses measured from GPC. Therefore, readers should not take the currently obtained exponents seriously because a set of narrowly distributed PVAc samples is certainly required to confirm those fitting parameters used in Figures 9 and 10. Note that studies of different common polymers, including

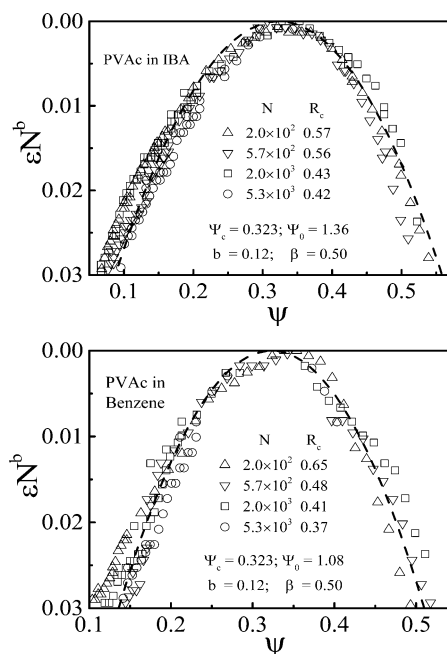


**Figure 10.** Symmetrized phase diagrams of four PVAc samples in isobutyl alcohol and in benzene by eq 2 with listed fitting parameters, where polymer volume fraction is converted  $\Psi$ , using eq 1, and  $\epsilon = (T_c - T_p)/T_p$ , reduced temperature.

polystyrene and PMMA, in different solvents are undergoing to check the values of those critical scaling exponents.

In principle, for a given polymer in different good solvents, the nature of each solvent only affects the prefactor in the scaling of various measured properties, such as the size, viscosity and translation diffusion coefficient, to the molar mass but not the scaling exponent. Here,  $\Psi_0$  is the prefactor. Therefore, using different values of  $\Psi_0$ , we should be able to scale two sets of a total of eight phase diagrams of four PVAc fractions in two different solvents into one master curve, which is exactly what we see in Figure 11. However, one has to note

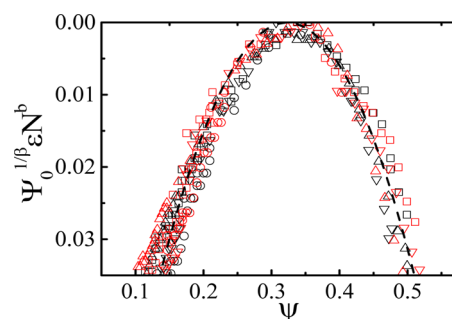


**Figure 11.** Symmetrized phase diagrams of four PVAc samples in two different solvents (black, isobutyl alcohol; red, benzene) by eq 2 with fitting parameters and symbols listed in Figure 10

that such a rescaling only works when the chain conformation remains. Using such a master curve, we will be able to construct the phase diagram of PVAc with a known molar mass in either benzene or isobutyl alcohol by measuring  $T_p$  of only one solution with a known concentration. We expect that for different linear polymers, if normalizing the molar mass of polymer chains by using the molar mass of a Kuhn segment (Kuhn length) instead of monomer’s molar mass, we would be

able to scale their phase diagrams into a master curve. The mapping of the phase diagrams of different linear polymers in solutions into a master curve is also undergoing.

## CONCLUSION

The newly developed microfluidic device used in the current study is readily applicable for the preparation of a series of small polymer solution droplets ( $\sim 200 \times 200 \times 400 \mu\text{m}^3 \approx 16 \text{ nL}$ ) with different well-controlled concentrations. The interchain association inside each of these droplets in the two-phase regime can be sensitively and precisely monitored by using a small-angle laser light-scattering (LLS) detector. A combination of such a series of polymer solution droplets and LLS enables us to quickly and accurately map the phase diagram of a polymer in a given solvent. Namely, the droplets provide the concentration axis ( $X$ -axis) while the droplet (concentration) range, in which the interchain association occurs, marks the two-phase regime so that the two boundary droplets (concentrations) lead to the two points on the coexistence curve ( $\phi_L$  and  $\phi_H$ ) for a given solution temperature. Using a small temperature step ( $0.1 \text{ }^\circ\text{C}$ ), we can map the entire coexistence curve and find the critical concentration and the critical temperature of a polymer in a solvent within hours instead of months and years used in the conventional ways. It can be envisioned that, by using such a novel method, we will be able to map the phase diagrams of most of polymer solutions to enrich our databases in polymer handbooks for practical applications. Note that the current study is mainly focused on the development of this novel method in the current study so that we are not able to use the current data to prove or disprove those existing theories used to rescaling our data. We are now working on different well-defined polymer samples with a much broad molar mass range in different solvents. A set of precisely mapped phase diagrams of different polymers in different solvents will finally enable us to validate some universal critical scaling exponents predicted by statistic physics for the critical phenomena.

## AUTHOR INFORMATION

### Corresponding Authors

\*(Y.S.) E-mail: shangguan@zju.edu.cn.

\*(B.Z.) E-mail: bozheng@cuhk.edu.hk.

\*(C.W.) E-mail: chiwu@cuhk.edu.hk.

### Notes

The authors declare no competing financial interest.

## ACKNOWLEDGMENTS

The financial support of the National Natural Scientific Foundation of China Projects (20934005 and 51173177), the Ministry of Science and Technology of China Key Project (2012CB933802), and the Hong Kong Special Administration Region Earmarked Projects (CUHK4042/10P, 2130241 and 2060405; CUHK4036/11P, 2130281 and 2060431; CUHK4042/12P and CUHK7/CRF/12G, 2390062) is gratefully acknowledged.

## REFERENCES

- (1) Koningsveld, R.; Kleintjens, L.; Geerissen, H.; Schuetzichel, P.; Wof, B. *Comprehensive Polymer Science: The Synthesis, Characterization, Reactions & Applications of Polymer*; Pergamon Press: New York, 1989.
- (2) Wild, L. *Adv. Polym. Sci.* **1991**, *98*, 1.
- (3) Koningsveld, R.; Stockmayer, W.; Nies, E. *Polymer Phase Diagrams: A Textbook*; Oxford University Press: New York, 2001.

- (4) Shultz, A.; Flory, P. *J. Am. Chem. Soc.* **1952**, *74*, 4760.
- (5) Gonzalez-Leon, J.; Mayes, A. *Macromolecules* **2003**, *36*, 2508.
- (6) Tong, Z.; Einaga, Y.; Miyashita, H.; Fujita, H. *Macromolecules* **1987**, *20*, 1883.
- (7) Mao, H.; Li, C.; Zhang, Y.; Bergbreiter, D.; Cremer, P. *J. Am. Chem. Soc.* **2003**, *125*, 2850.
- (8) Mao, H.; Li, C.; Zhang, Y.; Furyk, S.; Cremer, P.; Bergbreiter, D. *Macromolecules* **2004**, *37*, 1031.
- (9) Hansen, C.; Sommer, M.; Quake, S. *Proc. Natl. Acad. Sci. U. S. A.* **2004**, *101*, 14431.
- (10) Zheng, B.; Tice, J.; Roach, L.; Ismagilov, R. *Angew. Chem., Int. Ed.* **2004**, *43*, 2508.
- (11) Laval, P.; Lisai, N.; Salmon, J.; Joanicot, M. *Lab Chip* **2007**, *7*, 829.
- (12) Shim, J.; Cristobal, G.; Link, D.; Thorsen, T.; Jia, Y.; Piattelli, K.; Fraden, S. *J. Am. Chem. Soc.* **2007**, *129*, 8825.
- (13) Zhou, X.; Li, J.; Wu, C.; Zheng, B. *Macromol. Rapid Commun.* **2008**, *29*, 1363.
- (14) Ren, K.; Dai, W.; Zhou, J.; Su, J.; Wu, H. *Proc. Natl. Acad. Sci. U.S.A.* **2011**, *108*, 8162.
- (15) Shi, F.; Han, Z.; Li, J.; Zheng, B.; Wu, C. *Macromolecules* **2011**, *44*, 686.
- (16) Zheng, B.; Roach, L.; Ismagilov, R. *J. Am. Chem. Soc.* **2003**, *125*, 11170.
- (17) Duffy, D.; McDonald, J.; Schueller, O.; Whitesides, G. *Anal. Chem.* **1998**, *70*, 4974.
- (18) Wu, C.; Zhou, S. *Macromolecules* **1995**, *28*, 8381.
- (19) Tice, J.; Song, H.; Lyon, A.; Ismagilov, R. *Langmuir* **2003**, *19*, 9127.
- (20) Sanchez, I. C. *J. Appl. Phys.* **1985**, *58*, 2871.
- (21) Alpert, D. *Z. Phys. Rev. B.* **1982**, *25*, 4810.
- (22) Dobashi, T.; Nakata, M.; Kaneko, M. *J. Chem. Phys.* **1980**, *72*, 6685.
- (23) Xia, K. Q.; An, X. Q.; Shen, W. G. *J. Chem. Phys.* **1996**, *105*, 6018.